Diffusion-like drying of a nanoporous solid as revealed by Magnetic Resonance Imaging

Benjamin Maillet[1], Guido Dittrich[2], Patrick Huber[2, 3, 4], Philippe Coussot[1,*]

[1] Laboratoire Navier (Ecole des Ponts Paris Tech-Univ Gustave Eiffel-CNRS), Champs-sur-Marne, France

[2] Institute for Materials and X-Ray Physics, Hamburg University of Technology, Hamburg, Germany

[3] Center for X-Ray and Nano Science CXNS, Deutsches Elektronen-Synchrotron DESY, Germany

[4] Center for Hybrid Nanostructures CHyN, University Hamburg, Hamburg, Germany

* Author to whim correspondence should be addressed: Philippe.coussot@univ-eiffel.fr

Abstract: Drying plays a central role in various fabrication processes and applications of functional nanoporous materials, most prominently in relation to energy storage and conversion. During such processes liquid coexists with air inside the sample, leading to transport as a result of concentration gradients of vapor and/or liquid. Experimentally it is extremely challenging to unravel this transport phenomenology inside the hidden geometry of porous media. Here we observe drying of a model nanoporous material (monolithic mesoporous silica glass, Vycor) with Magnetic Resonance Imaging. We show that for various boundary conditions (air flux intensities) no dry region develops but the sample desaturates in depth. This desaturation is almost homogeneous throughout the sample for weak air flux, while saturation gradients can be observed for sufficiently strong air flux. We demonstrate that the transport of water is mainly ensured by liquid flow towards the free surface, resulting from a gradient of vapor pressure, associated with local saturation (via the desorption curve), and leading to a gradient of liquid pressure (via the Kelvin law). Assuming otherwise standard hydrodynamic characteristics of the nanoconfined liquid this results in a diffusion-like model which appears to represent the experimental data very well in terms of spatial distribution of water in time inside the sample for various boundary conditions (air flux intensities). Finally we have a predictive model of the detailed drying characteristics of a nanomaterial from the knowledge of its pore size, permeability and desorption curve. This provides new insight for rational design of drying-based processes employing functional nanoporous materials and for a mechanistic understanding of drying phenomenologies in natural nanoporous media.

I. INTRODUCTION

Water transport in nanoporous media plays a central role in many aspects of science and technology: shrinkage or cracks during drying of clay, nanocolloidal gel [1-2] or cement [3], moisture transfers in cementitious construction materials [4] and their impact on durability or building comfort and heating [5], hydrocarbon release in low-permeability reservoirs [6], sap flow in plants [7-8], synthesis and in -operando performance of the wide class of functional nanoporous materials [9-10]. Also, considering the latent heat associated with liquid-vapor transition, water sorption or desorption might constitute a source of energy storage or harvesting and is already of crucial importance in many technical cooling applications, most prominently cooling of electronic devices [10]. Also, capillary forces in pore space emerging upon drying can be used as bio-inspired mechanical actuation schemes [11-13].

The extraction of liquid from nanoporous systems can involve some liquid flow, but the nanofluidic behavior of liquids confined in nanopores is a subject of debate [14-15], the main questions being as to whether continuum fluid mechanics still applies when the pore scale is not much larger than the molecular size, and if viscous fluid properties are similar. One nanometer is considered as the critical size below which continuum

mechanics does not apply anymore but various specific effects can occur just above this limit [16]. For example, it was proposed that standard hydraulic laws apply if one takes into account a slipping [17] or a fixed molecular layer [18-20]. Also, the usual capillary imbibition process [21] was shown to follow the same rules at nanoscale [8, 22-23].

The desorption case is a priori more complex as now one can expect the coexistence of water and air in nanopores at different stages of the process, with questions on the interactions between the liquid, the vapor and the solid, and the resulting transport properties. More generally it questions the free surface hydrodynamics of liquid in nanopores [24-25]. So far, most studies focused on the evaporation from 1D or 2D nanoporous systems for which the liquid-air interface was fixed [26-28] or observable [29-31], so that the process could essentially be described by taking into account evaporation and vapor diffusion from relatively simple air-liquid interfaces. The drying of 3D nanoporous systems is directly connected to various applications, but its study also constitutes a stronger challenge due to the difficulty of internal visualization and of theoretical description of a two-phase flow through a complex medium.

During drying of real (3D) micro or macro porous media, pore-network effects occur that sensitively depend on geometrical parameters such as the aspect ratio pore length/pore diameter, tortuosity and interconnectivity [32-34]. However, usually they homogeneously desaturate [35-38]. This is due to dominant capillary forces, which increase when the pore size decreases, and which induce sufficiently fast equilibration of the water content (and thus, of the Laplace pressure) throughout the medium. Then, below some critical saturation (current liquid volume divided by the void volume in the absence of liquid, noted S) and air flux, a dry region develops from the free surface [38-40]. It is not clear whether similar effects can take place in nanoporous media as internal observations in such systems are scarce. Magnetic Resonance Imaging (MRI) of drying nano-colloidal gels (made of silica beads with radius down to 6 nm) under a single air flux nevertheless showed that some saturation gradient develops from the beginning of the experiments till the end but no dry region appeared [1, 38]. Thus, remarkably, such nanoporous samples are still able to desaturate in depth more or less like macroporous materials, but the exact physical origin and dynamics are not yet established.

Here we provide a rigorous analysis of drying of a nanoporous solid based on the analysis of NMR measurements giving detailed information on the local liquid content at any time during water extraction from a model nanoporous material under different conditions. Through a detailed theoretical description of the physical mechanisms, we finally show that the water transport is mainly ensured by liquid flow resulting from a gradient of vapor pressure, and assuming otherwise standard hydrodynamic characteristics, so that the whole process of extraction is very well described by a diffusion model with a diffusion coefficient which, as a first approximation, can be considered as constant.

II. MATERIALS AND METHODS

We used porous Vycor glass (*Corning glass*, code 7930), a virtually pure fused silica glass permeated by an isotropic, three-dimensional network of interconnected tortuous pores [41-42]. From nitrogen sorption isotherm the surface area was found to be 100 m^2/g, the average pore radius R=4.6 nm, and the pore volume 0.218 cm^3/g. For such materials the pore size distribution is generally narrow [43-44]. The aspect ratio of pore length to diameter lies between 5 and 7 and the sample porosity is $\varepsilon = 0.3$ [34]. The water sorption and desorption curves for such a material were provided in Gruener et al [23]. We used samples of main axis length 1.2 cm, and of section 4 x 6 mm.

For drying experiments we started by placing the dry sample in contact with distilled water, which ensures a full saturation. Then all the faces of the sample except one (its “free surface”) were covered with Teflon and the sample was submitted to a dry air flux along this free surface (see inset of Figure 1), which induces a transport of water along its main axis towards the free surface. The temperature was $21 \pm 1°C$. The drying

rate increases with the air flux intensity, which may be understood as a result of the decrease of the thickness of the (boundary) layer of exchange, through which the vapor has to diffuse to reach the dry region. As we will see later the most straightforward way to characterize the air flux is through this layer thickness (δ), which can be estimated from the initial drying rate, i.e. when the sample is saturated. The sample is inserted in a Bruker NMR minispec mq20, 0.5 T. We measured the transverse relaxation time T_2 of water protons using a Carr-Purcell-Meiboom-Gill (CPMG) sequence [45] with the main following parameters: number of scans: 256, echo time: 0.4 ms (i.e. less than the minimum T_2 for adsorbed water) and repetition time: 2 s, for a total measurement duration (for one T_2 distribution) of 5 min. Such data may be analyzed to obtain the probability density function (pdf) of the NMR relaxation time T_2, which we call the relaxation time distribution. The details of this technique and the physical interpretations have been described elsewhere [46-47]. Roughly speaking, for such small pores, the relaxation time is related to the mobility of water molecules. More precisely, according to the Brownstein and Tarr model [48], under the assumption of biphasic fast exchange, the relaxation time scales as the ratio of the volume of free liquid water to the area of the water-solid interface, with a factor depending on the interactions of the water molecules with the surface.

During the same tests it was also possible to get, with Spin Echo sequence, 1D NMR profiles of the water content with this NMR system equipped with a 4 T/m vertical pulsed gradient unit. These 1D profiles obtained by Fourier Transform represent the spatial distribution of water along the sample drying axis, each data point corresponding to the free water content in a cross-sectional layer of thickness equal to the spatial resolution. The main parameters used are: number of scans: 256, echo time: 7.2 ms, field of view: 20 mm, number of pixels: 128, and Repetition time: 2 s, for a total measurement duration of 5 min. However, in the present context, the profiles obtained from this standard procedure can be seen as qualitative because of the standard weighting of the signal amplitude in the spin-echo sequence by a factor $\exp -T_E/T_2$, in which T_E is the echo time and T_2 the most representative transverse relaxation time of the slice. In other words, the NMR signal in these profiles may be affected by the local relaxation, which is rather fast for water in such nanopores. The strong dependency of the relaxation time with the saturation (see below) allows to develop a de-weighting procedure to recover quantitative profiles (i.e. a local signal amplitude that is effectively proportional to the local water mass concentration). In that aim we used the straightforward correspondence between T_2 and the saturation in the case of a homogeneous desaturation of the sample under very slow drying conditions (see below), which allows to deduce the corresponding spin-echo weighting for each layer at each time during drying. Note that with this procedure, due to increasing noise for lower saturation, reliable data can be obtained only for a saturation larger than 0.25.

III. RESULTS AND DISCUSSION

General characteristics

A typical evolution of the relaxation time distribution during drying is shown in Figure 1. By integrating this distribution over the whole range of relaxation times we obtain the total NMR signal in time, from which we can deduce the average saturation (as the ratio of the current to the initial total NMR signal, i.e. $\overline{S}$) vs time curve for our different experiments.

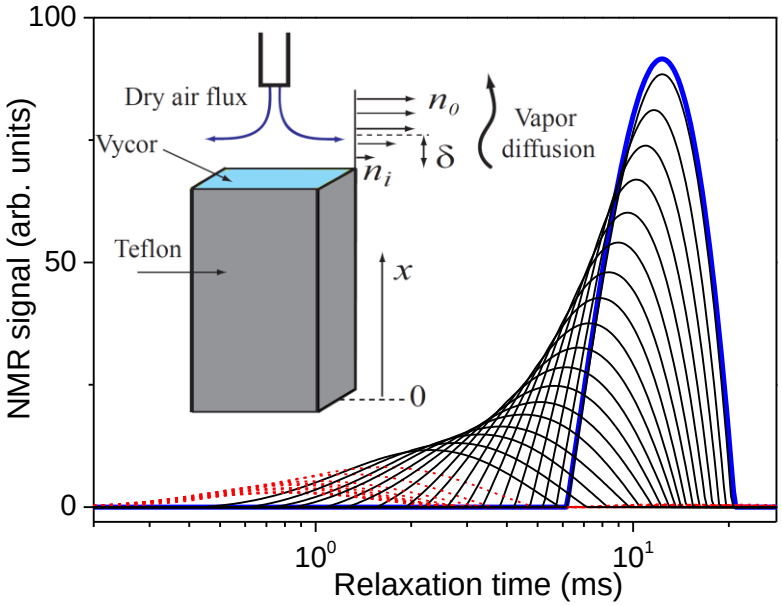

Figure 1. Relaxation time distribution for an intermediate air flux (see Materials and Methods) ($\delta = 8.5\mathrm{mm}$) at different times during drying: every 3 h (continuous black lines), then every 6 h (dashed red lines). The initial distribution is the thick blue line. The inset shows a scheme of the experiment.

The qualitative evolution of the relaxation time distribution are similar for all our experiments. The initial distribution, which corresponds to the sample saturated with water in liquid state, exhibits only one relatively narrow, symmetrical, peak situated around a relaxation time value of 12 ms. This single peak further supports the validity of the fast-exchange assumption [49], i.e. in which, thanks to self-diffusion, the water molecules reach the solid walls a large number of times during the NMR relaxation so that, according to the Brownstein and Tarr model [48] the relaxation time is proportional to the ratio of the liquid volume to the wetted surface area. Note that since the typical length of diffusion of a water molecule over a time duration of 12 ms is in the order of 10 microns, the relaxation time results from an exploration of the medium over a distance much larger than the pore size, and thus is related to the average volume to surface ratio well beyond the local heterogeneities. During drying, the amplitude of this peak decreases, as a result of the water content decrease, and simultaneously the peak shifts towards lower relaxation time. This is consistent with a fast-exchange situation in which essentially the liquid volume decreases while the wetted area does not vary significantly. More precisely, the average relaxation time of each distribution appears to evolve very close to the water content (see Figure 2), which exactly corresponds to the prediction of the Brownstein and Tarr [48] model assuming that the area of the solid-liquid interface remains essentially constant. Our observations thus demonstrate that the liquid wets most of the solid surface all along the drying process. Finally, the distribution approaches a peak centered around 0.9 ms. It may nevertheless be remarked that during the desaturation, there is also a progressive slight spreading of the peak, i.e. the width of the distribution increases, which suggests that some slight saturation heterogeneity also develops in the sample, leading to different T_2 in the different parts of the sample

It is worth noticing that in the last stage of drying the average saturation slowly but continuously decreases towards lower values. At the end of our experiment the saturation, which is still decreasing, has reached a value in the order of 7%. Assuming a homogeneous layer covering the solid surface this value equals the ratio of the specific area times the layer thickness to the pore volume. Under these conditions the mean thickness

would be 0.15 nm, about half the water molecule diameter. This suggests that in this stage there is only a partial coverage of the solid surface by water molecules.

It is also remarkable that when the sample in such a state is now placed again in contact with a liquid bath, which leads to a progressive imbibition, the initial peak located around 1 ms progressively disappears as the sample is invaded by water, while a peak appears at much larger relaxation time, say around 10 ms (see inset of Fig. 2), whose amplitude grows in time. This corresponds to the progressive penetration of water over time. Indeed, as soon as a pore is invaded by water, the water molecules initially adsorbed along the surface and exhibiting a short relaxation time are now just molecules among others in the pore; all the water molecules now take part to the fast-exchange process, leading to a single relaxation time, longer than that associated with surface relaxation.

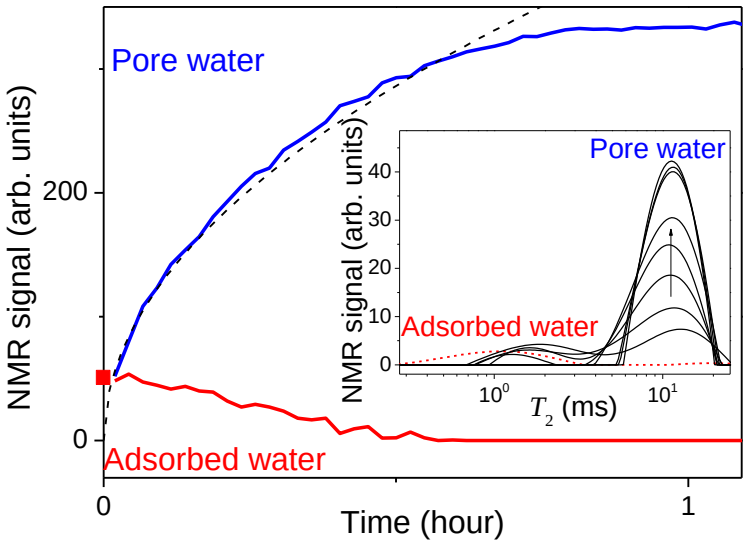

Figure 2: Imbibition of a Vycor sample: water mass (proportional to the NMR signal) associated with each region of relaxation time, i.e. below (adsorbed water) or above (pore water) 4 ms, as deduced from the integral of the probability density function in these ranges. The black dashed line is the Washburn model fitted to data (see text). The inset shows the distributions of transverse relaxation time at different times during imbibition (black curves from bottom to top): 3, 6, 11, 19, 32, 49, 66, 75 min. The red dotted line is the initial distribution (before imbibition).

We can further quantify this process through the integral of the pdf over the range of relaxation times including this growing peak, i.e. say between 4 and 25 ms. The curve of the resulting signal as a function of time is typical of a diffusion or capillary imbibition process [21], i.e. with a variation as function of the square root of time (see Fig. 2). Remarkably, the relaxation time of the pore water remains constant over time (see inset of Fig. 2). This confirms that the water invades the medium by progressively fully saturating a region of increasing thickness. This was also confirmed by MRI measurements of 1D water content profiles: see Appendix 1). This process in fact well corresponds to a capillary imbibition, as assumed in the Washburn model. The evolution of the signal associated with the initially adsorbed layer confirms this analysis: its amplitude progressively decreases as the signal of water at larger T_2 increases (see Fig. 2). Note that although it corresponds to the non-invaded region the adsorbed water signal does not seem to decrease with the square root of time, as expected from the above analysis. This is due to the uncertainty on the measurements for such a low signal amplitude, and the impact, on the Laplace transform used to get the pdf, of the close presence of a large peak associated with pore water.

Detailed drying characteristics

Differences in the drying characteristics appear when looking at the saturation vs time curves (see Figure 3). For sufficiently slow air flux, i.e. large δ (see definition below), the drying rate (i.e. water mass loss per unit time), proportional to the slope of the saturation vs time curve, remains constant down to low saturation, then progressively decreases (see inset of Figure 3). For stronger air flux there also exists an initial period of constant drying rate, but this period extends over a shorter range of saturations as the air flux is increased.

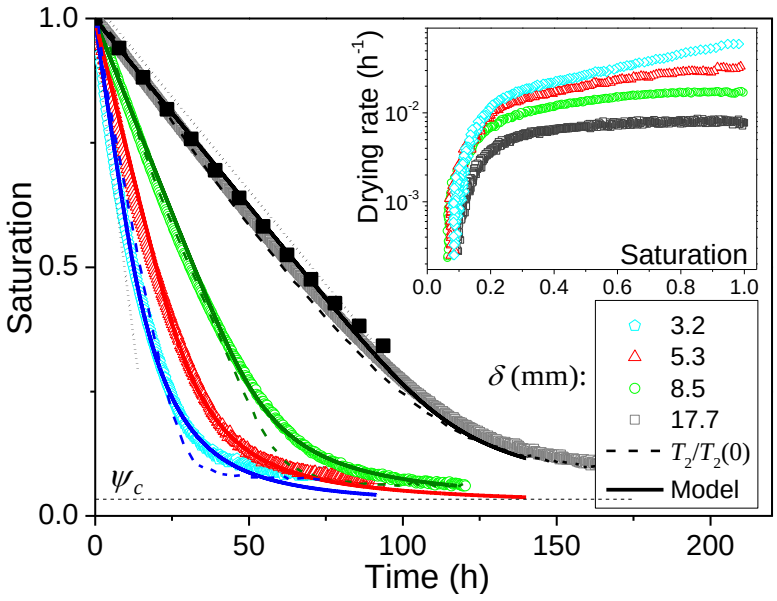

Figure 3. Total water content in time during Vycor sample drying under different air fluxes (resulting in different boundary layer thicknesses). The current to initial relaxation time ratio is represented for some tests (dashed lines). The black filled squares symbols correspond to the saturation computed from the 1D profiles shown in Figure 4a. The inclined straight dotted lines are guides for the eye. The inset shows the corresponding drying rate (saturation variation per unit time (in hours)) for the different tests (same symbols and colors).

These trends are associated with specific characteristics of the 1D profiles presented in Fig.4a. First note the consistency of these data with those extracted from the pdf: the saturation found by integration of the 1D profiles at different times corresponds to the saturation deduced from the integration of the distributions of relaxation time (see Fig.3). Also remark that these 1D profiles likely reflect a homogeneous situation in the radial direction. Indeed, significant edge effects are very unlikely, as they would hardly allow to get perfectly homogeneous desaturation down to low values as in Figure 4a: edge effects with different impact would occur at different depths in the sample, associated with different edge contexts.

For sufficiently weak air flux, rapidly after the beginning of the experiment, the 1D profiles exhibit a slight slope and then remain parallel to each other (see Figure 4a). Thus, remarkably, during drying (i) the nanoporous material starts desaturating in depth while its mean saturation has been only slightly decreased, and (ii) no dry region develops below the free surface.

This is reminiscent of drying characteristics of simple micro- or macro-porous systems, typically bead packings [38], clay [36] or cellulose [50] paste, for which the saturation was observed to remain perfectly uniform down to a value of 30% or lower. This results from capillary effects able to establish, by inducing liquid transport, a saturation equilibrium throughout the sample, sufficiently rapidly with regards to the drying rate imposed by

external conditions [51]. Note that in channels of a few tens of nanometers (i.e. sufficiently larger than the critical size of nucleating vapor bubbles [52]), instead of the standard air path propagation associated with capillary effects, cavitation was observed to be at the origin of a desaturation in depth (i.e. at some distance from the open surface of the sample) [52]. As for the standard capillary re-equilibration process, the air-liquid interface along the open surface of the sample remains almost the same. This situation allows to maintain a constant drying rate, as constant humidity conditions are maintained in the sample and in particular along its free surface (i.e., around 100%) from which the vapor diffuses. Moreover, for such simple micro- or macro-porous systems, when the liquid transport induced by capillary effects is not sufficiently fast with respect to the initially imposed extraction rate because now the permeability is too low [51], a dry region starts to develop from the free surface. Then the drying rate results from the vapor diffusion, from the liquid-air interface now situated inside the medium, to the free surface. Note that this is an "apparently dry" region, since the saturation is here generally appreciated with respect to the saturation in the main wet region. For example, a nano-layer of liquid molecules covering the solid surface in the "dry" region could hardly be detected with the technique used in such cases.

Here, we see that for a nanoporous medium, despite a very low permeability (it scales with the square pore size), an almost homogeneous desaturation is maintained down to low (mean) saturation, and no dry region develops. Such a result is likely general for a nanoporous medium with a connected pore network, since it was also obtained with silica bead packings for a single air flux and different bead sizes from 40 to 6 nm [38]. Moreover, here no clear dry region apparently tends to develop when the air flux intensity is increased: now the slope of the saturation distribution becomes steeper at the approach of the sample free surface, and the overall slope increases for stronger air flux, but the saturation still seems to tend to zero only at the approach of the free surface even after significant drying (see Figures 4b,c). This suggests that the dominant physical effects at play during the drying of a nanoporous material differ from usual effects taking place in porous materials with larger pores. More precisely there need to be stronger forces maintaining the liquid in contact with the solid, but also able to make it flow through the sample sufficiently rapidly.

Furthermore, looking more globally at the saturation distribution over time (see Figure 4) we can infer that these effects could lead to some diffusion process through the sample, resulting from some rate of extraction imposed at the boundary. Indeed, for a low rate of extraction, the liquid has time to almost uniformly distribute throughout the sample, but still some gradient of concentration should exist to induce a flow towards the boundary. For larger extraction rate, this gradient of concentration has to be larger and this effect is stronger at the approach of the region of liquid extraction.

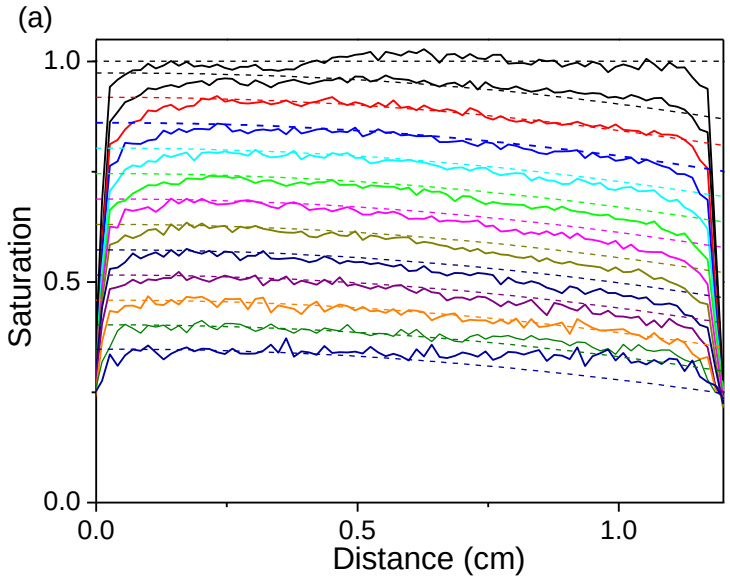

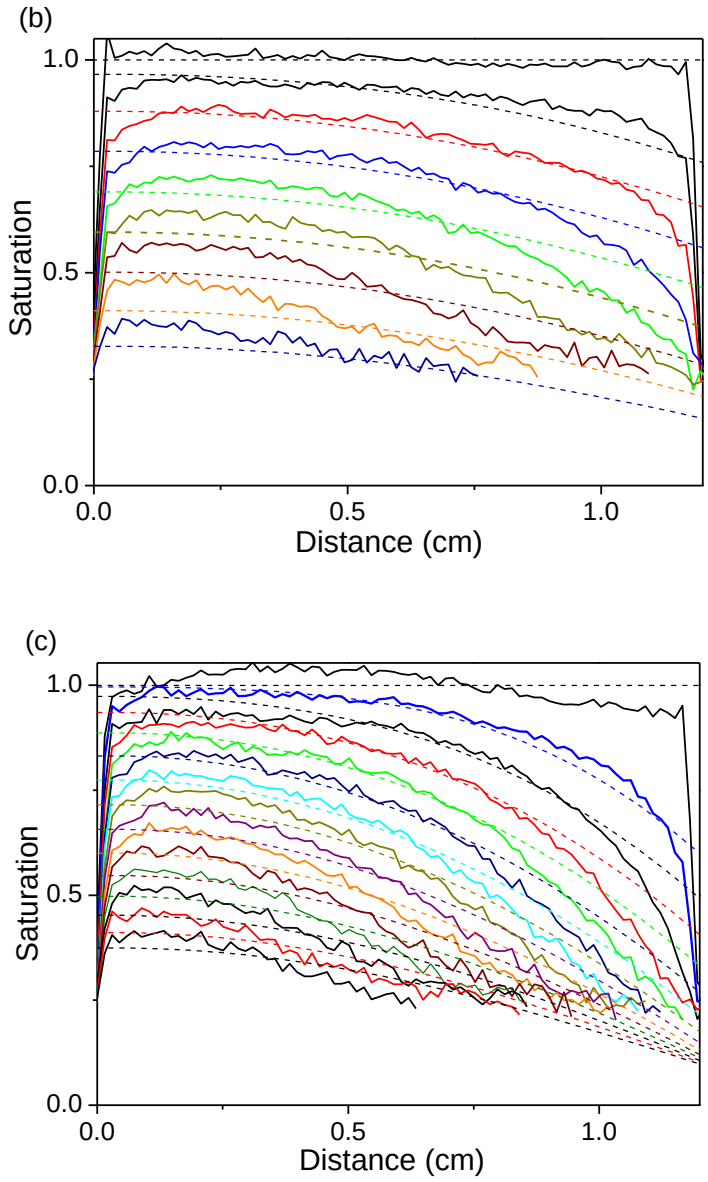

Figure 4. Saturation distribution (1D profiles) along sample drying axis at different times during drying with different air flux intensities: (a) $\delta = 17.7\,\mathrm{mm}$, profiles every 7.8 h; (b) $\delta = 8.5\,\mathrm{mm}$, profiles every 6 h; (c) $\delta = 3.2\,\mathrm{mm}$, profiles every 1.5 h, from initial time. Continuous lines correspond to NMR measurements, dashed lines to model predictions. Note that here the saturation was obtained by dividing the local NMR signal by the initial NMR signal averaged over the sample length.

Finally, if in addition we take into account both the above observations and studies on light [53-57] and neutron scattering [58] for a similar sample upon drying, we can conclude that the vapor phase invades according to an invasion percolation mechanism into the nanoporous medium, for which the interconnectivity of the pores plays an important role [59-60]. Additionally, a pore network study of the Kelvin effect for drying of mesoporous materials offers reasonable arguments for a rapidly equilibrated drying process with a homogeneous desaturation over time [61]. It is not sufficient for the humidity to be reduced below the pressure that drains a pore of a given radius; if this pore has also an unrestricted access via a percolation path

of empty pores to the surface, it can be emptied quickly. If it is blocked by smaller pores, it cannot drain until a sufficiently low value of humidity is reached to empty the narrowest blocking pores. As a result, the random connectivity leads to an interconnected, disordered network (or cluster) of drained pores. Additionally, consider liquid flow and the coexistence of menisci with different curvature and thus Laplace pressures. Menisci in large pore segments are receding, since they have a larger curvature radius and thus a smaller Laplace pressure counteracting the desaturation flux, i.e. the Laplace pressure at the small menisci. These clusters reach soon sizes on the order of the visible light length scale, i.e., fractions of a micrometer, so that strong light scattering is observable upon drying in the entire sample [53-57]. In fact, a detailed analysis of the light scattering allowed one to confirm predictions of the invasion percolation theory with regard to the vapor cluster geometries, most prominently the determination of their fractal dimension $d_f = 2.6$.

Of course, we have no direct evidences for this scenario, however, based on the rigorous neutron and light scattering analysis described above, we suggest for our drying geometry that percolating fingers of large empty pore clusters start from the surface and quickly reach the bottom of the sample, see the panel sequence (a) to (b) in Figure 5. In this propagating mode (regime I) a small saturation gradient from the top to the bottom is present. As soon as the invasion percolation fingers reach the sample bottom they rather laterally increase in size, so that a homogeneous desaturation of the sample takes place (see Fig. 5 c,d) until the sample is completely dry, except for a few monolayers of water adsorbed at the pore surface in the entire sample.

In the following we will describe theoretically the processes with the help of quantities which must be understood as averages over sample volumes much larger than these heterogeneities. Note that the above description in terms of percolating paths suggests that a similar phenomenon would take place during standard desorption experiment, so that, in fact, the desorption curve would not necessarily represent a homogeneous situation at a local scale.

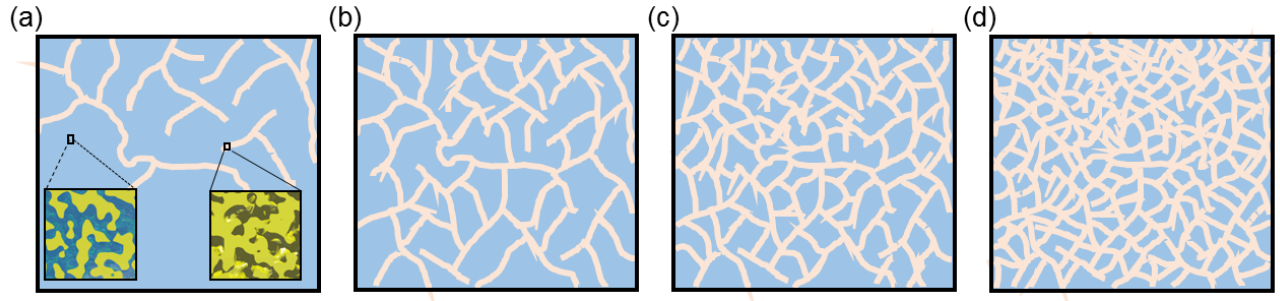

Figure 5: Illustration of the drying process in nanoporous silica glass. Invasion percolation clusters of partially empty pore segments (blue) propagate from the top to the bottom (a-b) through the saturated sample (yellow). Upon reaching the bottom the clusters increase homogeneously in size resulting in a homogeneous desaturation (c-d). The insets in (a) shows the detailed aspects of the structure at the pore scale (typical pore size about 10 nm) in the two different regions (empty or saturated). Please note that the illustration of the desaturation process represents the authors' naïve imagination of the invasion percolation process, as it has been rigorously shown to occur in drying of Vycor by light and neutron scattering experiments [53-57].

IV. MODELLING

Let us examine more precisely the physical effects taking place in this process, starting with the drying conditions imposed by the air flux. Drying occurs as a result of some unbalance between the humidity conditions inside the sample and the external conditions. Here the unbalance is maintained by the dry air flux

above the sample surface. Since the air flux can hardly penetrate the sample which is a finely divided dead-end network, the air essentially steadily flows along this surface. For such an air flow along a wet surface it may be shown, from the solution of the advection-diffusion equation, that along the normal direction above each point of the surface the gradient of RH (relative humidity, n) is almost constant, so that as a first approximation the vapor diffuses freely from the sample surface over a distance δ where it reaches the region where RH = n_0. The value of δ depends on the position along the sample surface, on surface shape and size and on the air flux characteristics. It is then natural to assume that a single average value δ, associated with given geometrical conditions, allows to represent the whole process of vapor transport above the sample surface [62-63]. It is worth emphasizing that, under these conditions, the drying rate results from the diffusion of vapor from the free surface, where the RH is equal to n_i, to the distance δ, where the RH is equal to n_0 (see inset of Figure 1); thus δ is independent of the water transport phenomena occurring inside the sample, and the drying rate depends on these phenomena only through the value n_i to which they lead. More precisely, according to Fick's law, in this boundary layer, the vapor flux, which is also the drying rate, may finally be written $J_0 = -\rho_0 D_0 \nabla n$, where $\rho_0 = 0.0185\ \mathrm{kg\,m^{-3}}$ is the saturation vapor density at our ambient temperature, $D_0 = 2.7\times10^{-5}\ \mathrm{m^2\,s}$ the coefficient of diffusion of vapor in air, and $\nabla n = \partial n/\partial x = (n_0 - n_i)/\delta$ (x being the distance along the direction of transport). δ can be directly estimated from the initial drying rate of the sample, since in that case n_i is known. Considering the desorption curve of Vycor sample, here n_i is initially equal to 1 but we have then a decrease of n_i towards 0.8 without significant change in saturation, so that finally the initial drying rate deduced from our data is essentially associated with $n_i = 0.8$. The values for δ indicated in this paper have been estimated in this way. Afterwards, i.e. during drying, the current drying rate will depend on the mechanism of water transport in the whole medium, leading to a value of n_i possibly varying in time.

Vapor transport

During drying the water is transported through the sample towards the free surface, and then diffuses in the form of vapor through the boundary layer. This internal transport can occur in the form of vapor diffusion or liquid flow. The vapor diffuses in the air network throughout the material as a result of some RH gradient ∇n. Since the pore size is smaller than the mean free path of water molecules ($l \approx 100\ \mathrm{nm}$ [64]), i.e. large Knudsen number (molecular regime), the diffusion coefficient is approximately $\varepsilon(1-S)D_v/\tau$ [64], in which τ is the tortuosity of the air network in Vycor ($\tau \approx 3.5$ [23, 65]), $\varepsilon(1-S)$ is the volume fraction of the air network, and $D_v = 2RD_0/2l$. The resulting mass flux writes $J_v = -\rho_0\left(\varepsilon(1-S)D_v/\tau\right)\nabla n$. Here, the gradient of n can be estimated from the 1D distributions of $S(x)$ and the desorption curve, assuming we have a local equilibrium situation, i.e. $n = n(\mathrm{S})$ at any time. This assumption seems realistic considering the very slow variations (slight changes of n over hours) of the local humidity in time during these drying tests. The validity of this assumption was checked in the case of cellulose fiber drying [63]. Notably, from our data the vapor mass flux estimated from the above equation appears to be much lower than the observed mass flux by a factor of several orders of magnitude. This means that the contribution of vapor flux due to the RH gradient inside the sample is negligible with regards to the vapor transport outside, in particular just above the sample top. This implies that most of the water supplied for the vapor transport in the boundary layer does not originate from vapor transport in depth in the sample, but rather comes from the liquid situated close to the free surface of the sample. As a corollary the water transport inside the sample mainly occurs in the form of liquid flow until the water reaches the sample top and finally evaporates.

Moreover, we do not have information about the contact between the Teflon and the Vycor sample but: i) a liquid layer of thickness significantly larger than the pore size cannot exist, as it could not be at equilibrium with the mean saturation in the sample, and the corresponding Laplace pressure (see below); ii) if a liquid

layer of significant thickness formed it would induce the presence of a small peak situated at larger T_2 in the pdf. Thus, if the contact between the Vycor is imperfect, and leads to the existence of some layer of thickness larger than the pore size, this layer is a priori filled with vapor. As a consequence, the water transport in this layer is associated with vapor transport, which can be estimated in the same way as for vapor transport through the porous structure (see above), so we can conclude it is negligible.

Liquid transport

The liquid motion in the porous medium results from some pressure gradient which comes from the gradient of saturation through the sample. For sufficiently large pore size this induces a gradient of Laplace pressure due to capillary effects as the meniscus size decreases for decreasing saturation [38]. Nevertheless, in that case although we know that the Laplace pressure increases when the saturation decreases, the exact theoretical relationship between these two variables is extremely difficult to establish from wetting characteristics and geometrical considerations. As a consequence we cannot predict exactly the rate of liquid transport due to capillary effects. The advantage of a nanoporous medium which saturates when submitted to a RH increased up to 100% is that, for a process like drying, during which the saturation decreases in time, the relationship between the pressure in the liquid and the saturation can be directly derived from the desorption curve, i.e., $\mathrm{S}(n)$ (see Fig. 6). Moreover, considering the slow variations of saturation in time (over hours), the local saturation and liquid-air interface are at equilibrium with the surrounding vapor at any time and position inside the medium. Indeed, since the velocity of vapor molecules is in the order of 400 m/s (as deduced from the expression of thermal energy as the mean kinetic energy of the particles) while the pore size is a few nanometers, the time needed for a vapor molecule to reach a liquid layer along a wall, is in the order of 10^{-11} s. This time is then also the characteristic time for an elementary exchange between vapor molecules and a molecule of the liquid phase. The volume of a pore being in the order of 4^3 nm^3, the maximum number of water molecules (of volume 0.34^3 nm^3) is $(4/0.34)^3$, i.e. in the order of 1600. The maximum time for complete exchange of the water molecules in the liquid phase is thus less than 10^{-11} s /1600, i.e. less than 10^{-8} s, which is well below the characteristic time of variation of the local saturation which derives from the characteristic time of drying (hours). This implies the equality between the pressure P_L in the liquid and the vapor water potential, i.e. $\left(\mathrm{R}T/\Omega_m\right)\ln n$, which gives the so-called Kelvin equation:

$$P_L = \left(\mathrm{R}T/\Omega_m\right)\ln n(S) \tag{1}$$

in which $\Omega_m = 18\,\mathrm{cm}^3\,\mathrm{mol}^{-1}$ is the molar volume of the liquid.

To describe the flow of the liquid network through the structure we can write the Darcy's law which relates the pressure gradient to the flow rate, i.e. $\nabla P_L = \mu V/k$, in which μ is the liquid viscosity, k the permeability of the medium and V the mean velocity through the structure (i.e. the ratio of the liquid flow rate per sample cross-section area). The permeability of the partially saturated medium may be expressed as $k = k_0 f(S)$, in which k_0 is the permeability of the saturated medium ($S = 1$) and f a function decreasing from 1 to 0 as S decreases to 0.

Taking the gradient of Laplace pressure into account the Darcy's law for the liquid network writes:

$$\frac{\mu}{k_0 f(S)} V = \frac{\mathrm{R}T}{\Omega_m}\nabla\left(\ln n(S)\right) = \frac{\mathrm{R}T}{\Omega_m}\frac{n'(S)}{n(S)}\nabla\left(S\right) \tag{2}$$

We deduce an equation for the water volume concentration in the sample, i.e. $\varphi = \varepsilon S$ where ε is the porosity, similar to Fick's first law: $V = = -D\nabla\phi$, with

$$D(S) = \frac{k_0 \mathrm{R} T f n'}{\varepsilon \mu \Omega_m n} \tag{3}$$

Fick's second law for ϕ , from which we directly get a diffusion-like equation for S (the mass flux being $J == -\rho D \nabla S$), states:

$$\frac{\partial S}{\partial t} = \nabla\left(D \nabla S\right) \tag{4}$$

Thus, we expect the drying characteristics to be the result of a process described by a non-linear, diffusion-like, transport equation, with an effective diffusivity coefficient depending on the local saturation value, and boundary conditions evolving with the saturation around the free surface as above described. Note that similar equations for unsaturated transport in porous media have been obtained, with analogous principles of derivation, e.g. the well-known Richards equation [66] or different approaches developed for cementitious materials [64], and for textiles [63] which take into account both vapor and liquid transport through porous systems. The specificity of our approach is the quantification of the Laplace pressure variations through the sorption curve.

Actually, we can estimate the value of the saturation-dependent factor fn'/n from the slope of the desorption curve and using a power-law model for the permeability of partially saturated porous media, i.e. $f = \left(S - S_c\right)^3 / \left(1 - S_c\right)^3$, in which ψ_c corresponds to some residual liquid layer. Here, in view of all our data we take $S_c = 0.035$ which appears to be the minimum saturation level reached during drying tests (see Figure 3), and thus would correspond to this residual liquid layer. Such an expression is the most frequently assumed in literature; it in particular corresponds to that proposed to represent a wide set of experimental data [67], and is close to various other theoretical expressions [68]. Moreover, it very well represents existing data for bead or granular packings (see [69]). One may remark that the structure of the Vycor porosity, which differs from that of a granular packing, might induce some different trends, but we are not aware of existing data for that system. However, the validity of the model for a wide range of materials, either monodisperse or polydisperse, thus exhibiting different porous structures, suggests it can reasonably be extended to Vycor structure. Finally, from the above mentioned data, we can suggest that the uncertainty associated with the use of this model, is less than 20% for a saturation higher than 0.4, but significantly increases as the saturation decreases to the critical value.

Under these conditions, it appears that despite the strong variations of n and f over the whole range of saturations the factor fn'/n remains approximately constant for S in the range of [0.1 – 0.8] (see inset of Figure 6), i.e. we have $fn'/n \approx 0.0145 \pm 35\%$. This means that a good approximation of the process can be obtained by using a constant diffusion coefficient in (3).

Besides, we can estimate k_0 from the imbibition test (see Fig. 2). Indeed, in that case we have a saturating front advancing in the medium, at a height h as a function of time t , given by the Lucas-Washburn model [21]: $h = 2\sqrt{k_0 t \sigma \cos\theta / \varepsilon R \mu}$, in which σ is the surface tension and θ the contact angle. Note that here we estimated the Laplace pressure to be due to a meniscus of radius R at any time, which is a critical simplification. We also assume perfect hydrophilicity, i.e. $\theta = 0$. This can be justified since the contact angle enters with the cosine into the Lucas-Washburn equation. Even if θ deviates from zero ($\cos\theta = 1$), a contact angle of up to 25°, as it has been reported for not specifically cleaned silica surfaces, would change the result of the cosine to a value 0.9 only. Fitting this curve to data assuming the sample top ($h = 1.2$ cm) is reached at the plateau of the NMR signal (see Fig. 2), we find: $K = k_0 \sigma / \varepsilon R \mu \approx 14.3 \times 10^{-9}$ $\mathrm{m^2 s}$, from which we deduce

$k_0 \approx 2.7 \times 10^{-19}\ \mathrm{m}^2$, with an uncertainty of the order of 2%. Such a value is consistent with previous observations based on gravimetrical imbibition experiments [42] on a similar Vycor sample leading to a hydrodynamic tortuosity of 3.6; the permeability can then be approximated by $k_0 = \frac{R^2\varepsilon}{8\tau}$ resulting in 2.2*10^{-19}, which is close to the value inferred in our analysis.

Finally, from (3) we get $D(S) \approx 1.8 \times 10^{-9}\ \mathrm{m^2 s^{-1}}$. Remarkably, this value is close to the also almost constant value obtained by Page et al [54] through a different approach for hexane desorption from Vycor.

The predictions of this simple model, i.e. equation (3) with the boundary conditions $J(x=H) = \rho_0 D_0 n_i(S)/\delta$ and $J(x=0) = 0$ can be computed by a simple finite-element method. Note that the solution could also have been expressed in an analytical form (see Crank, equation 4.53). In that aim we used an empirical model to represent the desorption curve (i.e. $n(S) = \left(1.3 + 0.0013 S^{-3.5}\right)^{-1}$) (see Figure 6). After adjusting the value of the effective diffusivity to a slightly lower value, i.e. $D = 1.3 \times 10^{-9}\ \mathrm{m^2\ s^{-1}}$, we observe an excellent agreement of these predictions with our data. This discrepancy between the theoretical and measured values of the diffusivity can come from the simplifying assumptions made concerning the wetting characteristics, i.e. the contact angle and the meniscus radius (see above), in the analysis of the imbibition process to estimate the (saturated) permeability. First of all, the whole set of drying curves, i.e. in a wide range of air fluxes, are well represented by the model (see Figure 3). Moreover, the theoretically calculated water distributions in time represent the data obtained under these different conditions very well and lead to either slight or strong saturation gradients (see Figure 4). Nevertheless, in some cases the slope of the theoretical profiles at the approach of the free surface is less prominent than it appears from data. This may find its origin in the uncertainty on the desorption measurements and the representation by a model, the error introduced in the model by assuming a constant diffusion coefficient, and in the uncertainty on the permeability function model. It seems difficult to elaborate further, in particular quantitatively, about the origin of this discrepancy. However we can add that despite this discrepancy all qualitative features are well predicted by the model under different air fluxes and, even more remarkable, the model predicts very well the drying rate over the whole range of saturation in any case (see Figure 3), which further supports its predictive nature.

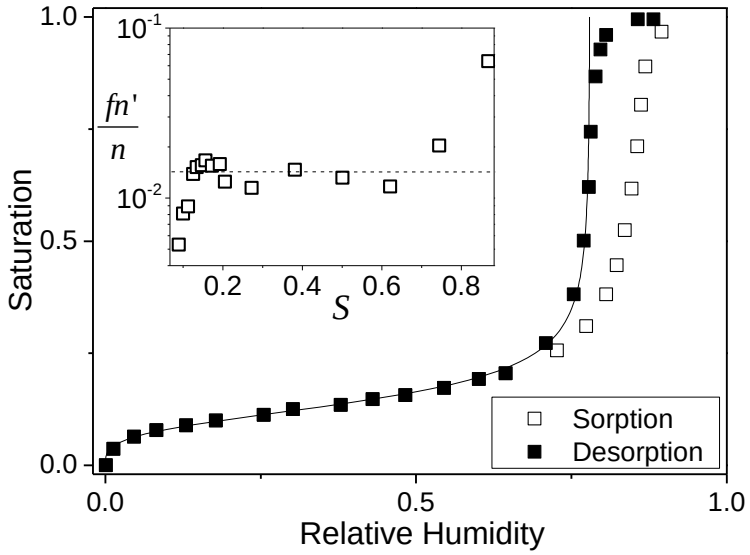

Figure 6. Water sorption and desorption curves of the Vycor sample. The inset shows the value of the saturation-dependent parameter of the diffusion coefficient computed from the

desorption curve and the empirical model for permeability of partially saturated porous medium.

V. CONCLUSION

Our results show that the water transport in the silica glass is mainly ensured by liquid flow resulting from a gradient of vapor pressure, and assuming otherwise standard hydrodynamic characteristics. The resulting simple diffusion-like model, assuming a constant effective diffusivity coefficient value, appears to very well represent the data in terms of spatial distribution of water in time inside the sample for various boundary conditions (air flux intensities) and at different saturations. This tends to validate our physical interpretation of the physics of drying of such a nanoporous medium, which can be generalized to other nanoporous media. For example, since the 1D profiles observed for a given air flux and beads of different nanometric sizes were similar [1, 38] we expect that the same modelling approach can be applied to granular packing too. Finally, we have a predictive model of the detailed drying characteristics of a nanomaterial from the knowledge of its pore size, permeability and desorption curve.

It is worth noting that our description is valid at a scale larger than the heterogeneities developing in the system, i.e. the probable air paths resulting from invasion percolation processes. This means that the desorption process does not take place homogeneously in all pores and we cannot see the desaturation and the resulting two-phase flow as taking place similarly in all pore sizes at the same time.

Let us remark that such results could be essential for applications in the field of energy: a good control and prediction of the water transfers inside the material allows to deduce, possibly with some coupling, the dynamics and distribution of thermal transfers in the medium, associated with latent heat, opening the way to a full physical approach of heat and mass transfers in nanoporous materials.

Acknowledgments

We acknowledge the scientific exchange and support of the Center for Molecular Water Science (CMWS). PH acknowledges funding from the European Innovation Council (EIC) under the European Union's Horizon 2020 research and innovation programme under grant agreement No. 964524 EHAWEDRY: “Energy harvesting via wetting-drying cycles with nanoporous electrodes” (H2020-FETOPEN-1-2021-2025).

Appendix 1: **1D profiles during imbibition process**

In Figure 7 we show the 1D profiles measured by the same MRI technique as for drying (see text). Here it is worth noting that the profiles correspond to the distribution of all water content in successive layers at increasing depth. As a consequence, in the bottom region, the water content includes the water in the bath in which the sample is partially immersed (see inset of Figure 7).

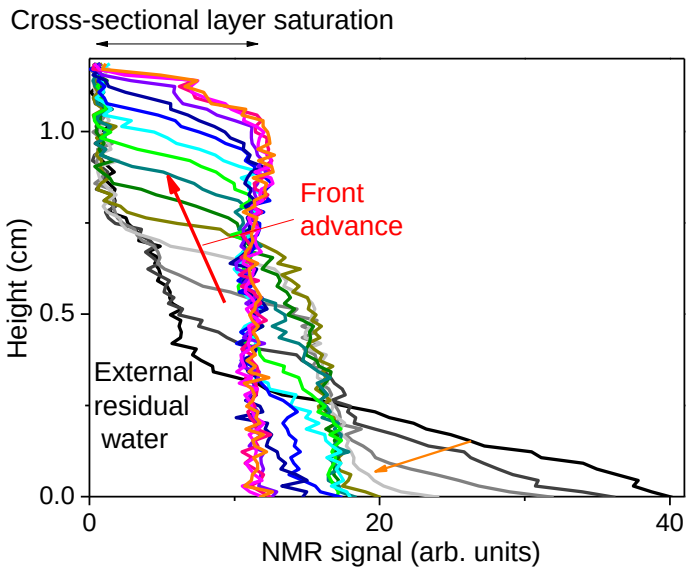

Figure 7: Successive 1D profiles (distributions) of water over time (every 150 s) along the axis of a Vycor sample initially dry and partially immersed in a water volume. Each data point at a given height corresponds to the total water content in the cross-sectional layer around this height. As a consequence, this includes the water inside the sample and the (external) water between the Teflon and the tube. As imbibition progresses a (slightly inclined front) associated with sample saturation advances upwards, while the volume of external water decreases. In the final stage, there is no more external water and the sample is saturated all along its height (vertical 1D profile). Note that for these tests the time schedule in the first times was not well controlled, and the adsorbed monolayer could not be observed due to its short relaxation time, which in our opinion precludes a detailed quantitative study of the process from such data in the present context.

References

[1] J. Thiery, S. Rodts, E. Keita, X. Chateau, P. Faure, D. Courtier-Murias, T.E. Kodger, P. Coussot, Water transfer and crack regimes in nanocolloidal gels, *Phys. Rev. E*, 91, 042407 (2015)

[2] J. Thiery, E. Keita, S. Rodts, D. Courtier Murias, T. Kodger, A. Pegoraro, P.Coussot, Drying kinetics of deformable and cracking nano-porous gels, *Eur. Phys. J. E,* 39, 117 (2016)

[3] S.D. Beyea, B.J. Balcom, T.W. Brenner, P.J. Prado, A.R. Cross, R.L. Armstrong, P.E. Grattan-Bellew, The influence of shrinkage-cracking on the drying behaviour of White Portland cement using Single-Point Imaging (SPI), *Solid State Nuclear Magn. Reson*., 13, 93-100 (1998)

[4] Y.P. Xi, Z.P. Bazant, L. Molina, H.M. Jennings, Moisture diffusion in cementitious materials – Moisture capacity and diffusivity, *Advanced Cement Based Materials*, 1, 258-266 (1994)

[5] M. Woloscyn, C. Rode, Tools for performance simulation of heat, air and moisture conditions of whole buildings, Building Simulation, 1, 5-24 (2008)

[6] B. Bao, J. Qiu, F. Liu, Q. Fan, W. Luo, S. Zhao, Capillary trapping induced slow evaporation, J. Petroleum Sci. Eng., 196, 108084 (2021)

[7] W. Shi, R.M. Dalrymple, C.J. McKenny, D.S. Morrow, Z.T. Rashed, D.A. Surinach, J.B. Boreyko, Passive water ascent in a tall scalable synthetic tree, Scientific Reports, 10, 230 (2020)

[8] O. Vincent, B. Marguet, A.D. Stroock, Imbibition triggered by capillary condensation in nanopores, Langmuir, 33, 1655-1661 (2017)

[9] P. Huber, Soft matter in hard confinement: phase transition thermodynamics, structure, texture, diffusion and flow in nanoporous media J. Phys. Condens. Matter, 27, 103102 (2015)

[10] A. Davoodabadi, H. Ghasemi: Evaporation in nano/molecular materials. Adv. Colloid Interface Sci. 290, 102385 (2021)

[11] I. Burgert, P. Fratzl, Actuation systems in plants as prototypes for bioinspired devices. Philos. Trans. R. Soc. A Math. Phys. Eng. Sci. 367, 1541–1557 (2009)

[12] G. Y. Gor, L. Bertinetti, N. Bernstein, T. Hofmann, P. Fratzl and P. Huber: Elastic response of mesoporous silicon to capillary pressures in the pores. Appl. Phys. Lett. 106, 1–13 (2015)

[13] R. Piotrowska, T. Hesketh, H. Wang, A. R. G. Martin, D. Bowering, C. Zhang, C. T. Hu, S. A. McPhee, T. Wang, Y. Park, P. Singla, T. McGlone, A. Florence, T. Tuttle, R. V. Ulijn and X. Chen: Mechanistic insights of evaporation-induced actuation in supramolecular crystals, Nat. Mater. 20, 403–409 (2021)

[14] L. Bocquet, E. Charlaix, Nanofluidics, from bulk to interfaces, Chem. Soc. Rev., 39, 1073-1095 (2010)

[15] U. Raviv, S. Giasson, J. Frey, J. Klein, Viscosity of ultra-thin water films confined between hydrophobic or hydrophilic surfaces, J. Physics Condensed Matter, 14, 9275-9283 (2002)

[16] N. Kavokine, R.R. Netz, L. Bocquet, Fluids at the nanoscale: from continuum to sub-continuum transport, Annual Review of Fluid Mechanics, 53, 377-410 (2021)

[17] P. Debye, R.L. Cleland, Flow of liquid hydrocarbons in porous Vycor, J. Applied Physics, 30, 843 (1959)

[18] B. Abeles, L.F. Chen, J.W. Johnson, J.M. Drake, Capillary condensation and surface flow in microporous Vycor glass, Israel J. Chemistry, 31, 99-106 (1991)

[19] J. Zhong, M.A. Alibakhshi, Q. Xie, J. Riordon, Y. Xu, C. Duan, D. Sinton, Exploring Anomalous Fluid Behavior at the Nanoscale: Direct Visualization and Quantification via Nanofluidic Devices, *Acc. Chem. Res.* 53, 347–357 (2020)

[20] O. Vincent, A. Szenicer, A.D. Stroock, Capillary-driven flows at the continuum limit, Soft Matter, 12, 6656 (2016)

[21] E.W. Washburn, The dynamics of capillary flow. *Phys. Rev*. **17**, 273–283 (1921)

[22] P. Huber, S. Grüner, C. Schäfer, K. Knorr, A.V. Kityk, Rheology of liquids in nanopores: A study on the capillary rise of water, **n**-Hexadecane and **n**-Tetracosane in mesoporous silica, Eur. Phys. J. Special Topics 141, 101–105 (2007)

[23] S. Gruener, T. Hofmann, D. Wallacher, A.V. Kityk, P. Huber, Capillary rise of water in hydrophilic nanopores, Phys. Rev. E, 79, 067301 (2009)

[24] B. Coasne, Multiscale adsorption and transport in hierarchical porous materials, New J. Chem., 40, 4078 (2016)

[25] K. Falk, B. Coasne, R. Pellenq, F.J. Ulm, L. Bocquet, Subcontinuum mass transport of condensed hydrocarbons in nanoporous media, Nature Communications, 6, 6949 (2015)

[26] Y. Akkus, Modeling of evaporation from nanoporous membranes using molecular dynamics simulation, Isi Bilim Ve Teknigi Dergisi-J. Therm. Sci. Technology, 39, 91-99 (2019)

[27] P. Jain, O. Vincent, A.D. Stroock, Adsorption, desorption, and Crystallization of aqueous solutions in nanopores, Langmuir, 35, 3949-3962 (2019)

[28] W. Shi, J. Vieitez, A.S. Berrier, M.W. Roseveare, D.A. Surinach, B.R. Srijanto, C.P. Collier, J.B. Boreyko, Self-stabilizing transpiration in synthetic leaves, ACS Applied Materials and Interfaces, 11, 13768-13776 (2019)

[29] Y. Li, H. Chen, S. Xiao, M.A. Alibakhshi, C.W. Lo, M.C. Lu, C. Duan, Ultrafast diameter-dependent water evaporation from nanopores, ACS Nano, 13, 3363-3372 (2019)

[30] Q. Xie, S. Xiao, C. Duan, Geometry-dependent drying in dead-end nanochannels, Langmuir, 33, 8393-8403 (2017)

[31] A. Jatukaran, J. Zhing, A.H. Persad, Y. Xu, F. Mostowfi, D. Sinton, Direct visualization of evaporation in a two-dimensional nanoporous model for unconventional natural gas, ACS Applied Nano Materials, 1, 1332-1338 (2018)

[32] D. Wallacher, N. Künzner, D. Kovalev, N. Knorr and K. Knorr: Capillary Condensation in Linear Mesopores of Different Shape. Phys. Rev. Lett. 92, 195704 (2004)

[33] R. Valiullin, S. Naumov, P. Galvosas, J. Kärger, H.-J. Woo, F. Porcheron and P. A. Monson: Exploration of molecular dynamics during transient sorption of fluids in mesoporous materials. Nature 443, 965–968 (2006)

[34] S. Gruener, Z. Sadjadi, H.E. Hermes, A.V. Kityk, K. Knorr, S.U. Egelhaaf, H. Rieger, P. Huber, Anomalous front broadening during spontaneous imbibition in a matrix with elongated pores, Proc. Nat. Acad. Sci. USA, 109, 10245-10250 (2012)

[35] J. Van Brakel, Mass transfer in convective drying. *Adv. Drying* **1**, 217-267 (1980)

[36] P. Faure and P. Coussot, Drying of a model soil, *Physical Review E,* 82, 036303 (2010)

[37] M.D. Seck, M. Van Landeghem, P. Faure, S. Rodts, P. Cavalier, R. Combes, E. Keita, P. Coussot, The mechanisms of plaster drying, *J. Mat. Sci.,* 50, 2491-2501 (2015)

[38] J. Thiery, S. Rodts, D.A. Weitz, P. Coussot, Drying regimes in homogeneous porous media from macro- to nanoscale. *Phys. Rev. Fluids* **2**, 074201 (2017)

[39] L. Pel, H. Brocken, K. Kopinga, Determination of moisture diffusivity in porous media using moisture concentration profiles, Int. J. Heat Mass Transfer, 39, 1273 (1996)

[40] G.H.A van der Heijden, L. Pel, H.P. Huinink, K. Kopinga, Moisture transport and dehydration in heated gypsum, an NMR study, Chem. Eng. Sci., 66, 4241 (2011)

[41] P. Levitz, Porous vycor glass: The microstructure as probed by electron microscopy, direct energy transfer, small-angle scattering, and molecular adsorption, J. Chem. Phys. **95**, 6151 (1991)

[42] S. Gruener, Rheology and Dynamics of Simple and Complex Liquids in Mesoporous Matrices, PhD thesis, Saarland University (2010)

[43] A.B. Shelekhin, S. Pien, Y.H. Ma, Permeability, surface-area, pore volume and pore-size of Vycor glass membrane heat-treated at high temperature, J. Membrane Sci., 103, 39-43 (1995)

[44] P. Levitz, Off-lattice reconstruction of porous media: Critical evaluation, geometrical confinement and molecular transport, Advances in Colloid and Interface Science, 76–77, 71-106 (1998)

[45] H.Y. Carr, E.M. Purcell, Effects of diffusion on free precession in Nuclear Magnetic Resonance experiments. *Phys. Rev.* 94, 630-639 (1954)

[46] H. Penvern, M. Zhou, B. Maillet, D. Courtier-Murias, M. Scheel, J. Perrin, T. Weitkamp, S. Bardet, S. Caré, P. Coussot, How bound water regulates wood drying *Physical Review Applied*, 14, 054051 (2020)

[47] T. Lerouge, B. Maillet, D. Courtier-Murias, D. Grande, B. Le Droumaguet, O. Pitois, P. Coussot, Drying of a Compressible Biporous Material, Phys. Rev. Applied, 13, 044061 (2020)

[48] K.R. Brownstein, C.E. Tarr, Spin-Lattice relaxation in a system governed by diffusion, *J. Magn. Reson.* **26**, 17-24 (1977)

[49] A. Valori, P.J. McDonald, K.L. Scrivener, The morphology of C-S-H: Lessons from 1H nuclear magnetic resonance relaxometry, Cement and Concrete Research, 49, 65-81 (2013)

[50] N. Ben Abdelouahab, A. Gossard, X. Ma, H. Dialla, B. Maillet, S. Rodts, P. Coussot, Understanding mechanisms of drying of a cellulose slurry by magnetic resonance imaging, Cellulose, 28, 5321-5334 (2021)

[51] P. Coussot, Scaling approach of the convective drying of a porous medium. *European Physical Journal B 15*, 557-566 (2000)

[52] C. Duan, R. Karnik, M.C. Lu, and A. Majumdar, Evaporation-induced cavitation in nanofluidic channels," Proc. Natl. Acad. U. S. A. 109, 3688 (2012)

[53] J. H. Page, J. Liu, B. Abeles, H. W. Deckman and D. A. Weitz: Pore-Space Correlations in Capillary Condensation in {Vycor}. Phys. Rev. Lett. 71, 1216–1219 (1993)

[54] J. H. Page, J. Liu, B. Abeles, E. Herbolzheimer, H. W. Deckman and D. A. Weitz: Adsorption and desorption of a wetting fluid in {Vycor} studied by acoustic and optical techniques. Phys. Rev. E 52, 2763 (1995)

[55] S. Ogawa and J. Nakamura: Hysteretic characteristics of 1/λ^4 scattering of light during adsorption and desorption of water in porous Vycor glass with nanopores. J. Opt. Soc. Am. A 30, 2079 (2013)

[56] S. Ogawa: 1/λ^4 scattering of light during the drying process in porous Vycor glass with nano-sized pores. J. Opt. Soc. Am. A 30, 154 (2013)

[57] S. Ogawa and J. Nakamura: Optically Observed Imbibition and Drainage of Wetting Fluid in Nanoporous Vycor Glass. J. Opt. Soc. Am. 32, 2397–2406 (2015)

[58] J. C. Li, D. K. Ross, L. D. Howe, K. L. Stefanopoulos, J. P. A. Fairclough, R. Heenan and K. Ibel: Small-angle neutron-scattering studies of the fractal-like network formed during desorption and adsorption of water in porous materials. Phys. Rev. B 49, 5911–5917 (1994)

[59] D. Wilkinson and J.F. Willemsen, Invasion percolation: a new form of percolation theory, J. Physics A: Mathematical and General, 16, 3365 (1983)

[60] M. Prat, Isothermal drying of non-hygroscopic capillary-porous materials as an invasion percolation process, Int. J. Multiphase Flow, 2, 875-892 (1995)

[61] O. Maalal, M. Prat, and D. Lasseux, Pore network model of drying with Kelvin effect, Physics of Fluids, 027103 (2021)

[62] M. Cocusse, M. Rosales, B. Maillet, R. Sidi-Boulenouar, E. Julien, S. Caré, P. Coussot, Two-step diffusion in cellular hygroscopic (plant-like) materials, *Science Advances*, 8, eabm7830 (2022)

[63] X. Ma, B. Maillet, L. Brochard, O. Pitois, R. Sidi-Boulenouar, P. Coussot, Vapor-sorption coupled diffusion in clothes revealed by MRI, Physical Review Applied, 17, 024048 (2022)

[64] J.F. Daian, *Equilibrium and transfer in porous media 1 – Equilibrium states*, Wiley, New York, 2014

[65] S. Gruener, D. Wallacher, S. Greulich, M. Busch, P. Huber, Hydraulic transport across hydrophilic and hydrophobic nanopores: Flow experiments with water and n-hexane, Phys. Rev. E, 93, 013102 *(*2016)

[66] L.A. Richards, Capillary conduction of liquids through porous mediums, Physics, 1, 318-333 (1931)

[67] S. Irmay, On the hydraulic conductivity of unsaturated soils, Transactions, Americal Geophysical Union, 35, 463-467 (1954)

[68] S. Assouline, D. Or, Conceptual and parametric representation of soil hydraulic properties: A review, Vadose J., 12, 1-20 (2013)

[69] R. Yang, E. Lemarchand, T. Fen-Chong, K. Li, Prediction of permeability of monodisperse granular materials with a micromechanics approach, J. Applied Geophysics, 127, 82-90 (2016)